Article:
Quintana-Nedelcos, A., Leong, Z. and Morley, N.A. (2021) Study of dual-phase functionalisation of NiCoFeCr-Alx multicomponent alloys for the enhancement of magnetic properties and magneto-caloric effect. Materials Today Energy, 20. 100621. ISSN: 2468-6069

https://doi.org/10.1016/j.mtener.2020.100621

Study of dual-phase functionalisation of NiCoFeCr-Alx multicomponent alloys for the enhancement of magnetic properties and magneto-caloric effect.

A. Quintana-Nedelcos,[1,a] Z. Leong,[1] N. A. Morley,[1]

[1]Department of Materials Science and Engineering, University of Sheffield, Sir Robert Hadfield Building, Mapping St., Sheffield, S1 3JD,

[a]a.quintana-nedelcos@sheffield.ac.uk

Abstract

We have studied the effect of phase separation on the magnetic and magneto-caloric properties of the $CoFeNi_{0.5}Cr_{0.5}$-Al_x (x= 0.0, 1.0 and, 1.5) system. Results show that a collaborative behaviour amongst FeCr-rich segregated nanoparticles (NPs) increases the saturation magnetisation (M_s) whilst the Curie temperature (T_c) is controlled by the amount of added Al. With a strong ferromagnetic coupling between segregated FeCr-NPs, the $CoFeNi_{0.5}Cr_{0.5}$-$Al_{1.0}$ sample shows the highest M_s (100 Am^2kg^{-1}) with an increase of 61% over the Al-free $CoFeNi_{0.5}Cr_{0.5}$ sample. It is argued that as the ferromagnetic interaction increases in a degenerated super-spin-glass like state of the NPs the field induced phase transition is broadened whilst the magnetic entropy decreases. In turn, the $CoFeNi_{0.5}Cr_{0.5}$-$Al_{1.0}$ sample shows the highest refrigerant capacity (17.1 Jkg^{-1} at $\mu_0\Delta H$ = 1.0 T), and the smallest measured magnetic entropy change (ΔS_m^{peak} = 0.22 $Jkg^{-1}K^{-1}$). We found that the enhanced magnetic and refrigerant capacity by mean of phase separation and NPs clustering are amongst the highest reported for the multi-component alloys being investigated for energy applications in the high temperature range.

Keywords

Magnetic properties; High Entropy Alloys; Multicomponent Alloys; Phase Segregation, Nano-Particles, Inter-particle Interaction; Magneto-caloric effect

Experimental

Synthesis: Samples of the stoichiometric composition of $CoFeNi_{0.5}Cr_{0.5}$-Al_x (x = 0.0, 1.0 and 1.5) were arc-melted at least three times in the presence of a Ti getter in an Edmund Buhler Compact Arc Melter using components of >99% purity. The samples were then cast into 6 mm diameter rods in a water-cooled copper hearth and were heat treated at 1423 K for 10 hours in Argon atmosphere, and quenched in water. Thereafter samples will be named as Al0.0, Al1.0 and Al1.5 for x = 0, 1.0 and 1.5, respectively.

Characterisation: A Thermo Fisher Scientific Inspect F50 (20 kV) was used for scanning electron microscopy (SEM) imaging. Energy dispersive x-rays (EDS) line scans were carried out at sites with distinct segregation. X-ray diffraction (XRD) using a Bruker D2 phaser, with Cu $K_{\square}$ source was for XRD characterisation.

Magnetic measurements: The vibrating sample magnetometer (VSM) module of a Quantum Design MPMS-3 system was used to determine the magnetic properties. Field-cooling (FC) and field-heating (FH) thermomagnetic $M(T)$ curves were measured for applied static magnetic fields ($\mu_0 H$) of up to 2.0 T at a heating (FH) or cooling (FC) rate of 5 K/min. Curie Temperatures were determined from the peak in the $\delta M(T) / \delta T$ *vs.* T plots. For the Magnetic Force Microscopy (MFM) images a Bruker's Dimension

XR NanoEC was used. Lift mode while tapping was used to obtain non-contact magnetic force images over the sample's area.

The magneto-caloric (MC) effect was studied by determining the temperature dependence of the magnetic field induced entropy change, $\Delta S_m(T)$, through numerical integration of the Maxwell relation from a set of magnetisation isotherms, $M(H)$. The standard thermal protocol for a second order phase transition (SOPT) was followed to measure each magnetisation isotherm by decreasing the temperature in steps of 5 K.

Introduction

As climate change progresses, calls for responsible actions to address the impact of modern life on our planet becomes more urgent. Solid-state magnetic refrigeration can be up to 30% more efficient than traditional gas compressor cooling technologies [1][2]; as such they are an emerging environmentally-friendly technologies that are re-writing the long-established technologies standards. Magnetic refrigeration relies on the magneto-caloric effect (MCE) which is observed in the so-called magneto-caloric (MC) materials. They are not yet commercially available as they require a wide list of criteria to be satisfied such as low-cost, scalable production process, mechanical stability, high thermal conductivity, high MCE and refrigerant capacity (RC) values, wide working temperature range, and sensitivity to low applied fields (1 T or less) [3][4][5]. This defines the complexity of the task from a materials engineering standpoint.

The isothermal magnetic entropy change (ΔS_m) in typical single Curie temperature (T_C) materials with first order phase transition (FOPT) or second order phase transition (SOPT) shows a "caret-like" shape with the highest value (ΔS_m^{peak}) at the Curie temperature, with higher values being more desirable. ΔS_m^{peak} values of FOPT materials are an order of magnitude higher than SOPT materials due to the concurrence of both a magnetic and crystallographic phase transition. However, there is a trade-off: thermal hysteresis leads to significant energy losses in the refrigeration cycle. FOPT materials also possess poor mechanical stability; the materials tend to fracture due to the stress induced (up to 4% volume change) during the crystallographic phase transition [6][7]. To date the preferred materials for magnetic refrigeration demonstrate SOPT. Commonly used MC materials in current magnetic cooling prototypes are Gd and LaFeSiH [2]. The high cost of the first, and the mechanical instabilities of the second are major obstacles for their upscaling to mass production. Alongside ΔS_m^{peak}, other figures of merit to evaluate the MC materials performance are the practical working temperature range and the refrigerant capacity (RC) [8]. As RC α ΔS_m^{peak} x δT_{FWHM}, increasing ΔS_m^{peak} and/or δT_{FWHM} increases heat transfer. For an ideal Ericsson refrigerant cycle the efficiency is maximised when $\Delta S_m(T)$ remains constant over the working temperature range [9]. As consequence, a "table-like" $\Delta S_m(T)$ shape is preferred over typical "caret-like" $\Delta S_m(T)$ shapes obtained in single T_C MC materials.

Multi-transitions MC materials is the most-used route to obtain a "table-like" $\Delta S_m(T)$ shape. T_C graded materials can be obtain either by stimulating a phase separation during the fabrication/post-annealing [1][10] treatment or by designing a composite of constituents each with a different T_C [2][11]. However, as ΔS_m and T_C tuning are highly sensitive to parameters such as elemental composition [7][12], microstructure variations [13][14], and post-annealing treatment [6][15][16], translating these experiments from a highly controlled lab-based research environment into a production line is an extremely difficult task.

Single-phase high entropy alloys (HEAs) belong to the wider family of multiphase near-equiatomic multi-component alloys (MCAs). The MCAs family have been intensively investigated due to their

unique combination of properties that can be beneficial for MC materials. The list includes high strength and hardness, corrosion and oxidation resistance, strong fatigue resistance and, high thermal stability, among others [17]. This combination of properties has started to attract some attention to the HEAs and MCAs and there is momentum on the investigation of them as potential active MC materials [18][19][20] (henceforth the term MCAs is used to encompass both HEAs and MCAs).

MCE in MCAs have been reported to be associated to the order-disorder magnetic SOPT. As such, characteristic ΔS_m^{peak} values are relatively low and therefore the enhancement of the RC relies on the widening of the working temperature range δT_{FWHM}. For example, Perrin *et al.* reported for $FeCoNiCu_{1-x}Mn_{1+x}$ ($0 > x > 0.1$) values of 0.115 $Jkg^{-1}K^{-1} > I\Delta S_m^{peak}I > 0.081$ $Jkg^{-1}K^{-1}$, 16.5 $Jkg^{-1} > RC=(I\Delta S_m^{peak}I \times \delta T_{FWHM}) >$ 9.6 $Jkg^{-1}K^{-1}$ and, 395 K > T_C > 264 K for applied fields ($\mu_0\Delta H_{max}$) = 0.55 T [19]. Belya *et al.* reported figures of $I\Delta S_m^{peak}I > 0.70$ $Jkg^{-1}K^{-1}$ and $RC=(\int_{T_{cold}}^{T_{hot}} -\Delta S_M\, dT) > 100$ $Jkg^{-1}K^{-1}$ at $\mu_0\Delta H_{max}$ = 5.0 T in NiFeCoCrPdx (x=0-0.5) MC materials [21]. As pointed by the authors, outstanding thermo-mechanical stability and corrosion and fatigue resistance makes them worthy to try. However, some common problems from the viability point of view to the most traditional MC alloys persist. For example, high-cost materials dependency (Pd), and an elevated compositional sensitivity ($FeCoNiCu_{1-x}Mn_{1+x}$, T_C = 395 K, 321 K, 297 K, 279 K, and, 264 K for x=0, 0.025, 0.05, 0,075, 0.1 respectively) [19].

In the present contribution we expand on preliminary results found in [22] where the FeCr-rich nanoparticles segregation dependence on Al addition in the $CoFeNi_{0.5}Cr_{0.5}Al_x$ system were systematically studied. For the current research, we investigate the impact on the magnetic and magneto-caloric properties of the functionalized $CoFeNi_{0.5}Cr_{0.5}Al_x$ system.

Discussion and analysis.

Context and brief summary of previous results.

We recently reported on the FeCr NPs phase segregation within AlNiCo rich matrix for $CoFeNi_{0.5}Cr_{0.5}$ with Al addition ($CoFeNi_{0.5}Cr_{0.5}$-Al_x, x = 0.0, 0.5, 1.0 and 1.5) [22]. The NPs-matrix segregation is driven by the addition of Al (Fig. 1), which is concomitant to a FCC ($CoFeNi_{0.5}Cr_{0.5}$) to BCC/B2 ($CoFeNi_{0.5}Cr_{0.5}Al_x$, x = 1.0 and 1.5) phase evolution (Fig. 2). We found two distinctive Curie temperatures (T_C) for the fully segregated $CoFeNi_{0.5}Cr_{0.5}$-Al_x ($x \geq 1.0$) samples, these are $T_C^{FeCr} > 850$ K and $T_C^{AlNiCo} < 700$ K respectively (*cf.* Table. 1). FeCr-NPs were found to have the greatest contribution to the total magnetisation in the Al1.0 and Al1.5 samples. The $CoFeNi_{0.5}Cr_{0.5}Al_{0.5}$ composition was identified as a transitional composition were both FCC and BCC structures coexist arising in a lath-like grain evolution rather than in a fully NPs-matrix segregation and therefore is not included in the present analysis. The jump in magnetisation occurring at T_C^{AlNiCo} is ≈ 5 times larger than the magnetisation change observed at T_C^{FeCr}. The result, however surprising at first sight, was objectively explained in the same paper. For the current analysis we use a phenomenological approach to expand on the previous explanation of the magnetisation jump at T_C^{AlNiCo} and theorise on how the dual phase functionalisation can be used for magneto-caloric materials development.

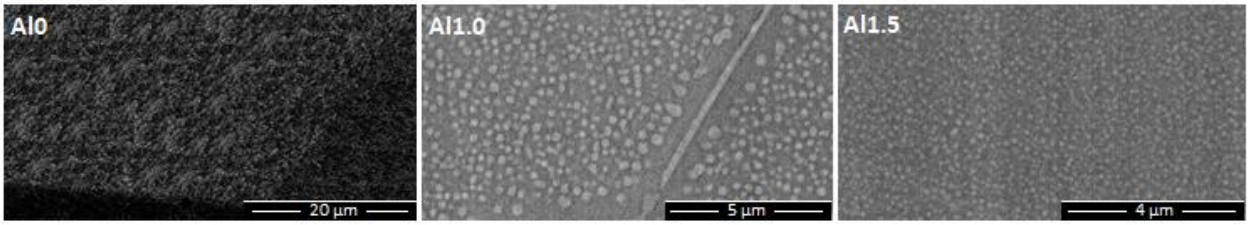

Fig. 1. SEM images of the $CoFeNi_{0.5}Cr_{0.5}$-Al_x samples, x = 0.0, x = 1.0 and x = 1.5.

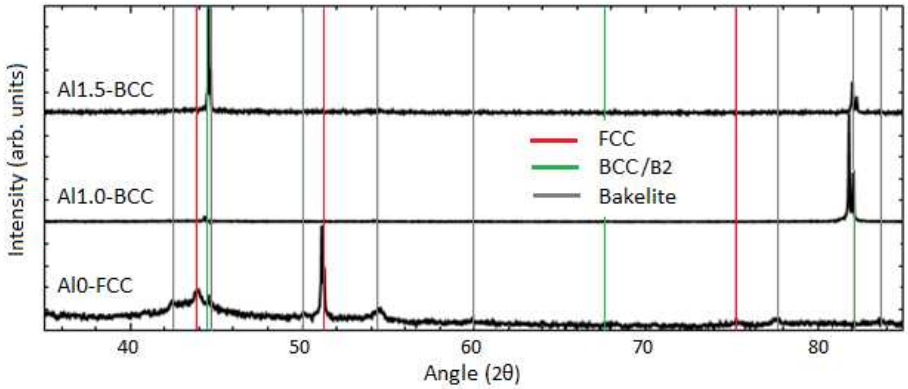

Fig. 2. XRD pattern of the $CoFeNi_{0.5}Cr_{0.5}$-Al_x samples.

Table. 1. Summary of main results obtained for samples Al0, Al1.0 and, Al1.5 in ref [22].

Property	Al0.0	Al1.0		Al1.5	
Magnetic-phase(s) (Tc-M(T))	265 K	640 K	905 K	455 K	825 K
Microstructural-phase(s) (SEM)	homogenous	Matrix	NPs	Matrix	NPs
Structural-phase(s) (XRD)	FCC	B2	BCC	B2	BCC
Chem. Comp. (EDS)	CoFeCrNi	AlNiCo	FeCr	AlNiCo	FeCr
Av. NPs' diameter <D> (SEM)	-	-	156 nm	-	90 nm
Std. Dev (<D>)	-	-	56 nm	-	32 nm
Av. inter-NPs' distance <d> (SEM) *	-	-	350 nm	-	168 nm
Std. Dev (<d>)	-	-	71 nm	-	27 nm

* <d> centre to centre distance calculated as the first peak (first nearest neighbours) of the RDF. RDF stands for the Radial Distribution Function (also known as pair correlation function) and provides the probability of finding a particle as function of the distance.

Analysis: NPs formation and magnetic properties.

Fig. 3(a) and fig. 3(c) show the FH and FC paths of the *M(T)* measurements obtained at different applied fields for the Al1.0 and Al1.5 samples. Both samples show a double magnetic transition. The transitions will be referred to as low temperature transition (LTT) and high temperature transition (HTT) where, LTT < 700 K (AlNiCo-rich matrix) and HTT > 800 K (FeCr-rich NPs) in both samples following previous analysis [22]. This is in agreement with the $M(H,T)$ data (Fig. 3., Fig. 4.) where the samples response to the change in field and temperature is similar. Any differences in T_C and saturation magnetisation (M_s) will be linked to differences in stoichiometric composition and to the NPs size and distribution.

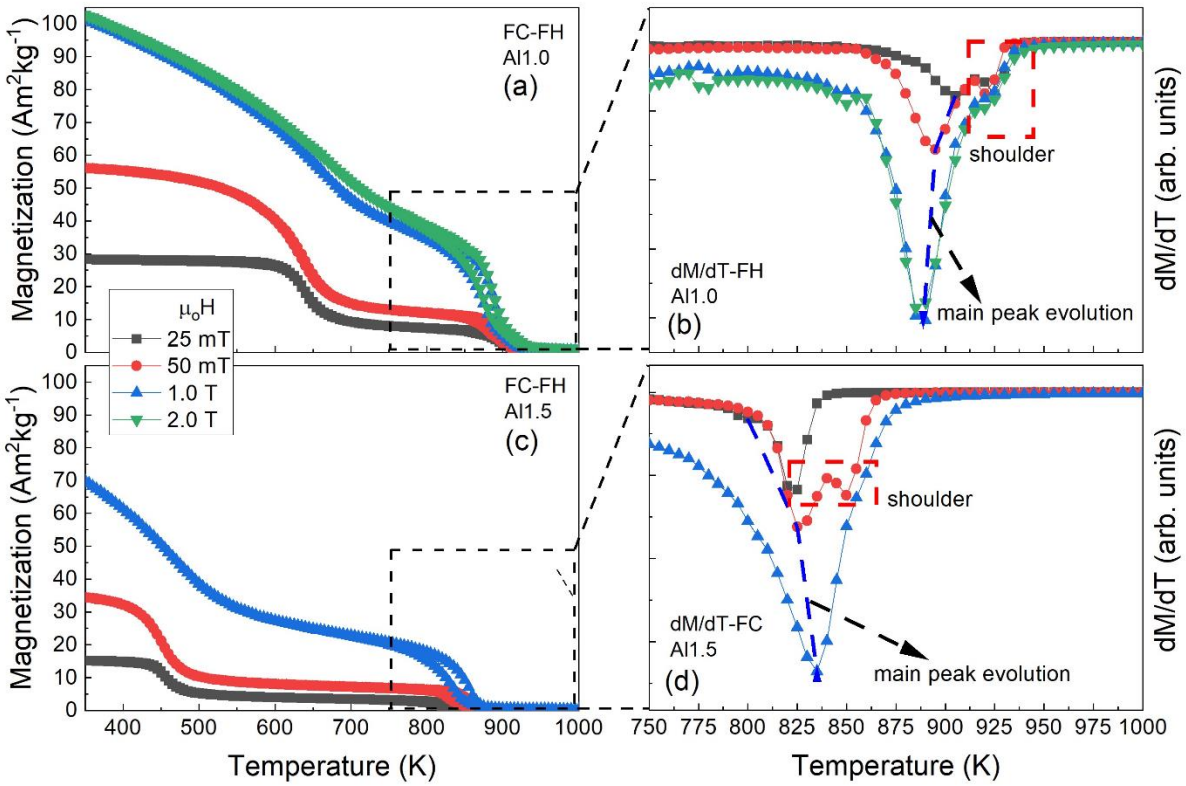

Fig. 3. FC-FH at different applied fields $\mu_0 H$ up to 2.0 T for sample Al1.0 **(a)** and sample Al1.5 **(c)**. dM/dT for the HTT region for sample Al1.0 **(b)** and sample Al1.5 **(d)**. Red dashed squares and blue dashed polylines are built to help the reader to follow the evolution of the shoulder and main peak respectively.

Both samples show a thermal hysteresis between the FC and FH paths at HTT, whilst there is a FC-FH overlapping at LTT. The result suggests that LTT is SOPT type whilst the thermal hysteresis at HTT demonstrates irreversibility. It has been reported that the precipitation and formation of FeCr nanoparticles occurs at T~HTT in $Fe_{78-x}Cr_xSi_4Nb_5B_{12}Ag_1$ [23] and $Fe_{73.5-x}Cr_xSi_{13.5}B_9Nb_3Cu_1$ [24] soft magnetic ribbons. The soft magnetic properties arises as the FM phase forms during the primary crystallisation (which includes the atomic segregation for the crystallisation to happen) and domain walls (DWs) might be pinned by other phases [24].

Calculations of the free energy of mixing indicate that the AlCoNi-rich matrix is always more negative than the solid solution phase for Al1.0 and Al1.5 even at elevated temperatures where entropy might stabilise the solid solution phase. As the solid solution phase is more negative than FeCr, AlCo and AlNi intermetallic formation in the AlCoNi rich matrix is expected to drive the formation of the FeCr nanoparticles. We would therefore expect the thermal hysteresis between the FC and FH path to be linked to the primary crystallisation of the FeCr NPs at HTT. Accordingly, the two transitions are observed for the Al:1.0 and Al:1.5 samples at HTT. For instance, fig. 3(b)[fig. 3(d)] shows an augmented image of the derivative of the FH-path of the magneto-thermal measurements at different fields for sample Al1.0 [Al1.5]. Notice the appearance of two minimums in the HTT region, which might be linked to a crystallisation process where the FeCr-NPs DWs are pinned to other phases [24].

In sample Al1.0 (fig. 3(b)) the peak observed at T=925 K correspond to the dominant phase for applied fields of $\mu_0 H \leq 25$ mT. The same remains almost unchanged and is displayed as a shoulder for $\mu_0 H \geq 25$ mT , as a new peak at a lower temperature starts to develop and increases in magnitude as the applied

field is increased. This "low-T" phase (presumable associated to the FeCr-rich phase) within the HTT region becomes the dominant phase for $\mu_0 H$ above 25 mT. A similar evolution of relative dM/dT peaks intensity with applied field within the HTT region is observed in the Al1.5 sample (fig. 3(d)). However, in the latter, there is a shift towards higher temperatures of both dM/dT peaks with applied field whilst, in the Al1.0 sample the shoulder-peak remains unchanged, with the dominant peak shifting to lower temperatures. Thereafter it is assumed that in the HTT region, FM-NPs stabilise within the AlNiCo-matrix. Henceforth, the correlated-phases formed at HTT is referred to as a single-FM-FeCr-rich-phase and the reported measured and calculated values as T_C and, $M(T,H)$, are those corresponding to the dominant phase at high fields. The Curie temperature at LTT T_C^{LTT} of the Al1.0 (Al1.5) sample is 640 K (455 K) and was calculated as the minimum of the derivative of the FC-path of the $M(H)$ curve obtained at 25 mT (fig. 5(d)). Likewise, T_C^{HTT} = 905 K and 825 K for Al1.0 and Al1.5 samples, respectively.

The FeCr-rich phase, T_C^{HTT} decreases with increasing Al concentration (Al1.0 →Al1.5). We previously identified two possible reasons for this: 1) The phase is not purely FeCr, but there is a small change in the stoichiometry within the nanoparticles and 2) The size of the FeCr grains/particles decreases with increasing Al concentration and this causes the decrease in the T_C [22]. We also find that differences in the shape and size of the HTT transition can be linked to the NPs size: After the completed HTT ($\mu_0 H$ = 25 mT) Al1.5 sample sees a jump in magnetisation of about 3 Am^2kg^{-1}, which is less than the half of the jump of 7 Am^2kg^{-1}observed in Al1.0 sample. The extent of the HTT transition (*E-HTT*, measured as the temperature window where the FC and FH paths are split) are *E-HTT* = 60 K and *E-HTT* = 110 K for Al1.5 and Al1.0 samples, respectively. Thus, for the larger NPs (Al1.0) to form at HTT a wider temperature transition, at higher temperatures is needed but, a higher magnetisation is achieved accordingly.

AlNiCo alloys are a well-known class of high-hard-magnetic materials were Al, Ni, and Co elements are alloyed to other elements such as Fe and Cu [25]. The hard magnetic properties arises due to the spinodal decomposition of the alloy into nano-precipitates of a FM FeCo-rich (α) phase within a non/weak-magnetic AlNi-rich matrix during cooling [25][26][27]. For instance, with a T_C > 1000 K, the coercivity of commercial Alnico 5-7 ($Fe_{49.9}Co_{24.3}Ni_{14.0}Al_{8.2}Cu_{2.3}Nb_{1.0}$), Alnico 8 ($Fe_{30.0}Co_{40.1}Ni_{13.0}Al_{7.1}Cu_{3.0}Ti_{6.5}$), and Alnico 9 ($Fe_{35.5}Co_{35.4}Ni_{13.1}Al_{7.0}Cu_{3.2}Nb_{0.5}Ti_{5.0}$) permanent magnets are as high as 59 kAm^{-1} (740 Oe), 151 kAm^{-1} (1900 Oe) and 109 kAm^{-1} (1375 Oe), respectively [26]. In contrast, from the M-H analysis at different temperatures (fig. 4) our materials show a soft-magnetic behaviour after every transition (insert of fig. 4) including for T < LTT (T_c^{AlNiCo}). The results are, however, consistent with what is expected for an AlNiCo-rich matrix, as a disordered Fe-Al and Co-Al pairings will show ferromagnetic order only if the Fe accounts for more than 40 at. % and the Co is larger than 50 at. %, respectively [28]. Whilst the Ni-Al pair do not show any magnetic order independently of the composition [28]. Assuming that most of the Fe segregates with Cr to form the NPs, the remaining composition of the matrix is then $Al_{35}Ni_{20}Co_{45}$ and $Al_{40}Ni_{16}Co_{44}$ for Al1.0 and Al1.5 samples, respectively. As such, in absence of Fe-Co and Fe-Al strong FM pairs, the weak-FM and dilute Co-Al pair will provide the main FM contribution to the AlNiCo-rich matrix. Therefore, it is fair to assume that the NPs are within a weak magnetic (WM)-AlNiCo-rich matrix. Thus, the FM-NPs account for the majority of the magnetism of the system. LTT dependence on stoichiometric composition of the matrix was discussed in [22].

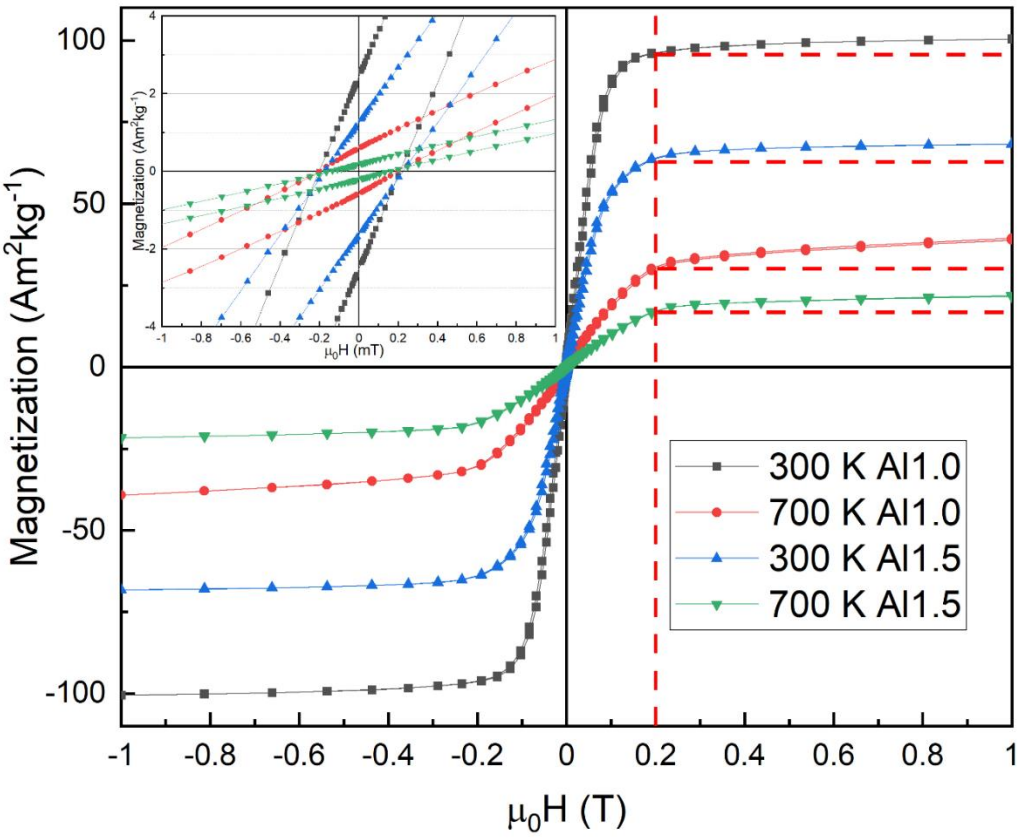

Fig. 4. Hysteresis loops at 300 K and 700 K for samples Al1.0 and Al1.5, inset: zoom in of the hysteresis loops for the low field region. Red Dashed lines are given for visual aid.

Hysteresis loops taken at T = 300 K < LTT and LTT < T = 700 K < HTT are shown in fig. 4. As with the *M(T)* measurements, the jump in magnetisation that occurs at LTT in fig. 4 is higher than the jump in magnetisation measured at HTT. ΔM(Al1.0, 1.0 T, M(1000K)-M(700K)) = 39 Am^2kg^{-1} whilst ΔM(Al1.0, 1.0 T, M(700K)-M(300K)) = 61 Am^2kg^{-1}. Likewise, ΔM(Al1.5, 1.0 T, M(1000K)-M(700K)) = 22 Am^2kg^{-1} whilst ΔM(Al1.5, 1.0 T, M(700K)-M(300K)) = 46 Am^2kg^{-1}. As the transition at LTT was successfully identified with the FM transition of the AlNiCo-matrix [22], this forms a weak magnetic phase that cannot explain the jump in magnetisation at LTT by itself. Therefore, the counterintuitive interpretation of the results might only arise if we naively assume that the whole magnetisation change at LTT is solely ascribed to the FM-transition of the AlNiCo-rich matrix. Moreover, from the hysteresis loops shown in fig. 4 we can observed that intrinsic properties of our materials such as coercivity field $H_c \approx 1.6$ kAm^{-1} (at $\mu_0 H_c$ = 2 mT) and saturation field $H_s \approx 159$ kAm^{-1} (at $\mu_0 H_s$ = 0.2 T) are fairly similar after both transitions. Thus, the magnetic ground state is stablished after completion of the HTT transition. Therefore, shifts of LTT and changes in the magnetisation saturation will be linked, mainly, to the Al concentration and to the size and distribution of the FeCr-NPs, respectively.

Although, 159 kAm^{-1} is identified as the saturation field (H_s), the magnetisation does not asymptotically approach the M_s value as expected for a pure FM transformation. Instead, the magnetisation continues to increase with a linear slope for $\mu_0 H > \mu_0 H_s$ as an antiferromagnetic/paramagnetic (AFM/PM) component (fig. 4) would do. The non-FM contribution appears in both samples at T < HTT.

The saturation magnetisation at 300 K and 1.0 T is M_s = 100 Am^2kg^{-1} and 70 Am^2kg^{-1} for sample Al1.0 and Al1.5, respectively (fig. 3(a), fig. 3(c), fig. 4 and, fig. 5(c).). A possible explanation for the decrease

in M_s with aluminium addition is due to the PM character of Al. However, the explanation would not satisfactory clarify the pronounced increased in M_s on the initial Al addition if we compare both Al1.0 and Al1.5 samples with the reference sample with no added Al. M_s (Al0.0) = 62 Am^2kg^{-1} at 50 K and 20 Am^2kg^{-1} at 300 K (> T_C) and 1.0 T, for instance, see fig. 5(c).

With PM-Al addition, the magnetic properties of the Al0.0 sample are considerable enhanced, enlarging the FM region (fig. 5. *i.e.* shifting T_c for more than 170 K towards higher temperatures) and, increasing M_s by 61 % and 16 % for Al1.0 and Al1.5 additions, respectively. For instance, the high M_s = 100 Am^2kg^{-1} shown by sample Al1.0 is similar or better than others systems considered of excellent magnetic properties, for example, AlNiCoFe [29], AlNiCo5 doped $Sm(Co_{0.9}Cu_{0.1})_5$ ribbons [30], $FeCoNiAlCr_x$, x = 0.1, 0.3, 0.5, 0.7, and 0.9 [31], $Fe_{38}Co_{38}Mo_8B_{15}Cu$ [32]. A high T_c, T_C^{LTT}(Al1.0) = 685 K, with high M_s and a low core losses as consequence of the low coercivity are attractive properties for industrial applications like sensors development, transducers and, transformers.

Analysis: NPs and cluster like behaviour.

The critical radius between the superparamagnetic state and a ferromagnetic state (R_S) for a single particle and, the radius at which the nanoparticle changes from a single FM state to a multi-magnetic-domain state (R_C) were calculated to determine whether Al1.0 and Al1.5 samples' NPs are either superparamagnetic or FM of single or multi-magnetic-domains. Equation 1 for R_S calculation can be deduced from $KV = k_BT$ whilst R_C was determined using the equation 2.

$$R_S = \sqrt[3]{\frac{3k_BT}{4\pi K}} \qquad \text{(equation 1)}$$

$$R_C = \frac{36\sqrt{AK}}{\mu_o M_S^2} \qquad \text{(equation 2)}$$

where μ_0 is the permeability of free space, and M_s was taken as the saturation magnetization for the FeCr NPs at 700 K, 39 Am^2kg^{-1} (298 kAm^{-1}) for Al1.0 and 22 Am^2kg^{-1} (168 kAm^{-1}) for Al1.5. A is the exchange stiffness of the FeCr NPs, and K the anisotropy constant. The used value of 2.28E-11 Jm^{-1} for A was estimated as the 95% of the reported exchange stiffness for pure Fe [33], as it has been stated that Cr addition of up to 30% to $Fe_{1-x}Cr_x$ bulk alloys decrease the Fe exchange stiffness by only 5 % [34]. K was estimated by using the equation 3 for which the anisotropy field (H_k) was determined from the magnetisation hysteresis loops at 700 K, by taking a straight line through the data around the origin and determining the field at the point where the line significantly diverge from the hysteresis loop. By following this conservative approach, H_k was approximated to 68 kAm^{-1} (at $\mu_0 H_k$ = 85.5 mT) for both samples.

$$K = \frac{\mu_o M_S H_k}{2} \qquad \text{(equation 3)}$$

Therefore, it was determined that NPs are mono-magnetic-domain-FM as R_S < 7 nm for both samples and the critical radius is R_C = 174 nm for Al1.0 sample and R_C = 411 nm for the Al1.5 sample. Thus, as much as 2x and 9x larger than the corresponding NPs average radius. Notice that the difference in estimated R_C values between Al1.0 and Al1.5 samples is solely ascribed to the variation in M_s which, as will be discussed in the following section, is consequence of the interparticle interactions. In an ideal system with no interacting NPs, M_s will be lower and R_C even higher than the calculated values. The mono-magnetic-domain-FM character of the NPs was confirmed via the MFM images shown in fig. 6.

For groups of mono-magnetic-domain NPs, it has been established that, the magnetic behaviour of the cluster depends on the temperature and the externally applied field. Such interparticle

interactions can be either long-range AFM dipolar force type or, based on nearest neighbours FM exchange coupling [35] [36] [37]. As both interactions are different in nature, the prevalence of one over the other will be determined by their relative strength. For instance, interparticle interactions nature and strength depends on, the single particle anisotropy and energy barrier E_B, the random distribution of easy axes, topological disorder, the NPs' arrangement, volume distribution and the magnetic properties of the spacer (interparticle medium) [35] [38].

If the interparticle interactions are negligible, magnetisation reversal of single particles of volume, V are governed by their own E_B, independent on whether or not E_B is modified by the presences of quasi-localised fluctuations modes associated to a weak interaction [38]. Therefore, the overall behaviour of these NPs cluster is as a superparamagnet (SPM) [38].

On the other hand, extended fluctuations modes linked to the strongest particle-particle interactions promote the formation of a collective state where the energy of the particle assembly is of greater significance, such that the individual E_B are not possible to be identified any more [38]. The transition from a particle self-governing E_B to the interdependent modify energy barrier can be trigger by, for example, an interparticle distance decrease, a spacer that enhances the exchange interaction, or, by a decrease of the thermal energy component of the system. As a consequence, the properties of the system are no longer relevant to the SPM state, making even more complex the prediction of an ordering temperature [38] [39].

For a sufficiently close arrangement of particles and, depending on the relative strength between competing dipolar and exchange interactions a ''nanoparticle replica of the spin-glass state, SG'' or, for instance, a super-spin-glass state (SSG) can form [35] [36] [38]. For example, it have been theoretically predicted that polydisperse ensembles of particles of different size favour the formation of glass states [40]. Highlighted similarities of the collaborating-NPs-cluster and traditional SG are (i) disordered arrangement of particles, (ii) random distribution of easy axes, (iii) presence of FM and AFM interaction due to exchange and dipole interactions [36], arising in disorder and frustration as short-range local order is revealed [38]. Furthermore, considering a broad distribution of size and interparticle-distance, a degenerate magnetic states is likely to form [40], which in turn will induce a gradual transition from a SPM to a SSG-like state [35] [39]. With an extended strength of interactions beyond the local clusters, the long-range collective superferromagetic SFM state can be achieved [35].

Analysis: NPs - cluster like behaviour, T ≥ LTT.

For temperatures above LTT, magnetic dipolar interactions are expected to dominate the interparticle interactions in detriment of the exchange coupling as the matrix is PM. Values of the magnetic dipole interaction energy (E_d, equation 4) at 700 K and critical temperature (T_0, equation 5) were calculated (results are shown in Table 2) in order to estimate the strength of the dipolar interaction between NPs and the critical temperature below which interacting NPs' magnetic moments increases the magnetic order of the sample.

$$E_d \approx \frac{\mu_0 \mu^2}{4\pi d^3} \qquad \text{(equation 4)}$$

$$T_0 \approx \frac{E_d}{k_B} \qquad \text{(equation 5)}$$

Where, μ_0 is the permeability of free space, μ is the single particle's moment ($\mu = M \times V$, with M being the magnetization, and V the volume of the particle), k_B is the Boltzmann's constant, and d the average interparticle distance [39].

Table. 2. Calculated E_d and T_0 at T = 700 K and $\mu_0 H$ = 0.0 T, 25 mT and 50 mT for Al1.0 and Al1.5 samples.

Al1.0	0.0 T	25 mT	50 mT	**Al1.5**	0.0 T	25 mT	50 mT
$\boldsymbol{\mu}$ (Am^2)	9.10E-18	1.36E-16	2.27E-16	$\boldsymbol{\mu}$ (Am^2)	5.83E-19	1.45E-17	2.91E-17
$\boldsymbol{E_d}$ (J)	1.93E-22	4.35E-20	1.21E-19	$\boldsymbol{E_d}$ (J)	7.16E-24	4.47E-21	1.79E-20
$\boldsymbol{T_o}$ (K)	14.00	3149.60	8748.88	$\boldsymbol{T_o}$ (K)	0.52	324.11	1296.44

Both samples show relatively high values of μ and E_d. For example, dipolar exchange energy between NPs of Fe_3O_4 of circa 11 nm diameter and $d \approx 13$ nm was found to be ≈ 4.36E-22 J at room temperature [41], and ≈ 8.28E-22 J for CoFe3 particles of 7.6 nm diameter [42]. In particular, Al1.0 sample shows enough interparticle dipolar interaction energy to overcome the thermal energy, k_BT, at temperatures as "high" as 14 K at remanence, and more than 3000 K at applied fields as low as 25 mT, quite above the temperature range of study and the melting point of the material. On the other hand, Al1.5 sample has, for $25 \leq \mu_0 H \leq 50$ mT, an interacting/non-interacting T_0 transition temperature between 324 K and 1296 K. With a decrease in d (Table 1) and a fairly similar Fe:Cr composition, the considerable decreased E_d with Al addition should be ascribed to the smaller volume of NPs in Al1.5 sample and the derived lower magnetic moment of the NPs (Table 2).

From previous results it can be suggested that at T ≥ LTT, Al1.0 sample shows a strong dipolar interparticle interaction, favouring a SSG state in detriment of the SPM state [39] whilst in Al1.5 sample both states coexists, being the SSG more relevant as the field increases. Further evidence of this conclusion can be obtained from the non-equilibrium character of the SSG-phase and its properties dependence on the thermomagnetic history [43].

For systems in thermomagnetic equilibrium, where the transition will always follow the same path, both isofield and isothermal measurements probe the same phenomenon [44]. However, for NPs clusters, where the thermal and the field-induced reversal of the magnetisation can be tuned independently a difference between the isofield and isothermal measurements [35] can be expected. Therefore, a comparison between the direct (FC/FH) and indirect (MT) magnetisation dependence on temperature *M(T)* measurements can give valuable insights on the magneto-thermal history of a system.

In order to study the magnetisation dependence on the thermo-magnetic history for T ≥ LTT, the direct and indirect *M(T)* curves in the Al0.0, Al1.0, and Al1.5 samples were measured and compared. The Al0.0 sample has no Al addition and shows a single FCC structure with a single standard second order phase transition SOPT below room temperature (RT) [22]. Fig. 5. shows the *M(T)* curve obtained from the FC-FH direct measurement and indirectly (MT) from the magnetisation dependence on field *M(H)* virgin loops. Both, indirect MT and direct FC-FH *M(T)* curves where taken on 5K steps and at 25 mT, 50 mT and 1.0 T.

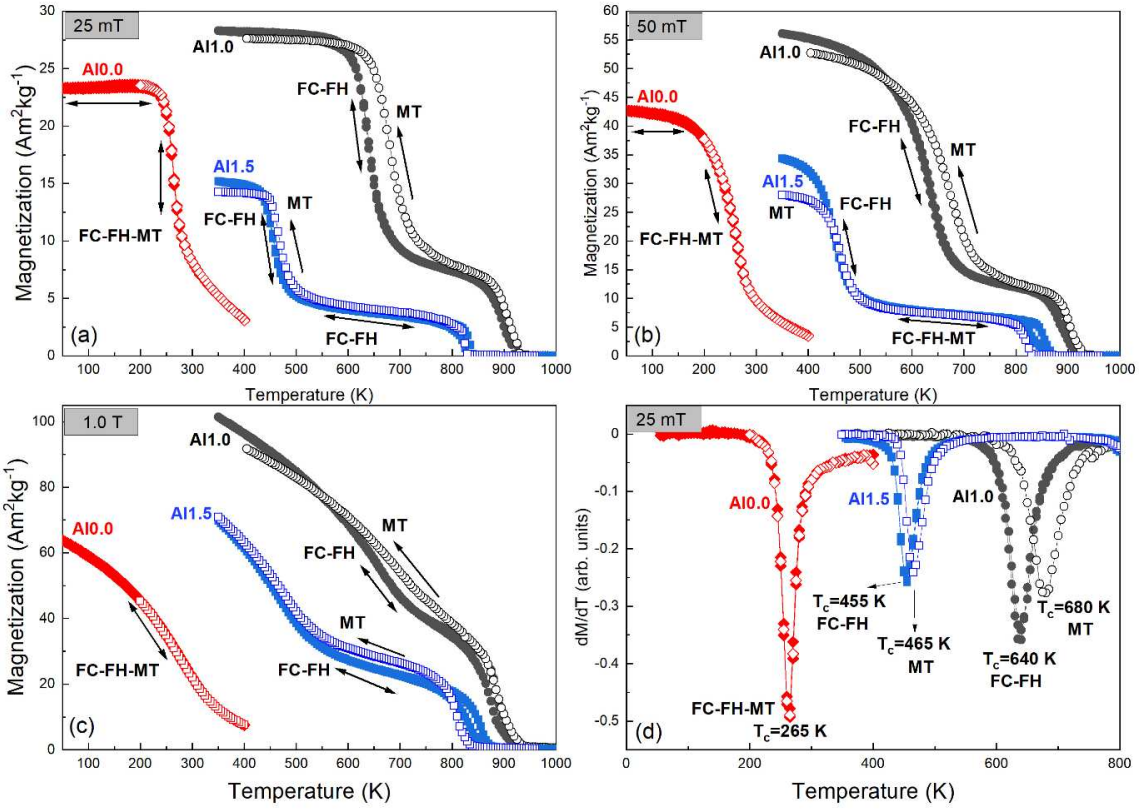

Fig. 5. FC-FH path of direct *M(T)* measurements curves (solid symbols) and the indirect magnetisation dependence on temperature (MT) curve obtained from isothermal measurements of virgin loop in a decreasing temperature path (open symbols) for samples Al0.0 (**red**), Al1.0 (**black**) and Al1.5 (**blue**) at applied fields of 25 mT **(a)**, 50 mT **(b)** and 1.0 T **(c)**. **(d)** *dM/dT* of the FC-FH and MT curves in the LTT temperature window.

As expected for a SOPT, there is an overlapping between the FC-FH and MT curves of the Al0.0 sample. However, with the addition of Al and the corresponding NPs-matrix segregation in Al1.0, there is a significant difference between the FC-FH curve and the MT curve, with the MT curve being at higher temperatures. This difference in the temperature curves then decreases to an almost neglected FC-FH – MT separation with further Al addition (Al1.5). In accordance to [35], this suggests that NPs clusters for the region LTT < T < HTT are more liked to happen in the Al1.0 sample than in the Al1.5 sample. Therefore, considering a broad distribution of size (Table. 1) and interparticle-distance of NPs in Al1.0 sample, a degenerated magnetic states with commons characteristics to a SSG-like state is likely to form within the LTT < *T* < HTT region [35][40]. As a consequence of the enhanced magnetic ordering, the Al1.0 sample achieve higher magnetization values compared to the Al1.5 sample of smaller and weakly-interacting NPs. Note that the term weakly-interacting and not non-interacting NPs is used for sample Al1.5 as a small, yet measurable, difference between the FC-FH – MT curves is observed (fig. 5(d)), accordingly to the dipolar interaction analysis. However, due to the weak interparticle interaction, overall behaviour of the NPs cluster is closer to the SPM type [38] for the Al1.5 sample.

Analysis: NPs - cluster like behaviour, T < LTT.

As the samples go through the LTT temperature region, changes in NPs interaction and cluster formation are expected. Size and configuration of the clusters obey the local equilibrium between dipolar and exchange interactions, but now, the latter is enhanced by the magnetic-bias provided by

the WM matrix. As the WM matrix provides a magnetic medium that enhances the exchange interaction, the AFM-like symmetry achieved under a predominant dipolar interaction breaks into a favoured FM-like short range interactions between NPs. The "bridging" mechanisms have been reported for AlNiCo materials where FM-FeCo-rich nano-precipitates align antiferromagnetically within the PM-AlNi-rich matrix [26]. In the later, it was also demonstrated that, for a FM coupling of the NPs, an exchange-bridge, where the bridge's domain wall energy is equal to the coupling energy of NPs is needed. For instance ferromagnetically-coupled NPs of FeCo and FeCr have been achieved in Cu-made exchange-bridge [26] and Cu substrate [45], respectively.

Fig. 6. shows the MFM image of the magnetic phase configuration for the Al1.0 sample at room temperature (RT << LTT)). The bright and dark regions denote the areas of the highest magnetisation with an antiparallel alignment respect to each other. Images of a total surface area of 20 µm x 20 µm (fig. 6(a) and fig. 6(b)) and 5 µm x 5 µm (fig. 6(c) and fig. 6(d)) correspond to the Al1.5 (fig. 6(a) and fig. 6(c)) and Al1.0 (fig. 6(b) and fig. 6(d)) samples.

From the MFM images, a labyrinth structure of magnetic domains is observed. The most obvious difference between the samples is the width and length of the stripes. For the Al1.5 sample, the magnetic domain stripes can be as thick as 0.5 µm, 4-5 times the average NPs' diameter(<D> = 90 nm ± 32 nm) and more than 6 µm long. Whilst for the Al1.0 sample, the stripes' width and length are of the order of 1 and 3-5 times (< 1 µm) the particle's size, (<D> = 156 nm ± 56 nm), respectively. Making, on average, stripes width and length of sample Al1.0 less than one six the size of the stripes of sample Al1.5.

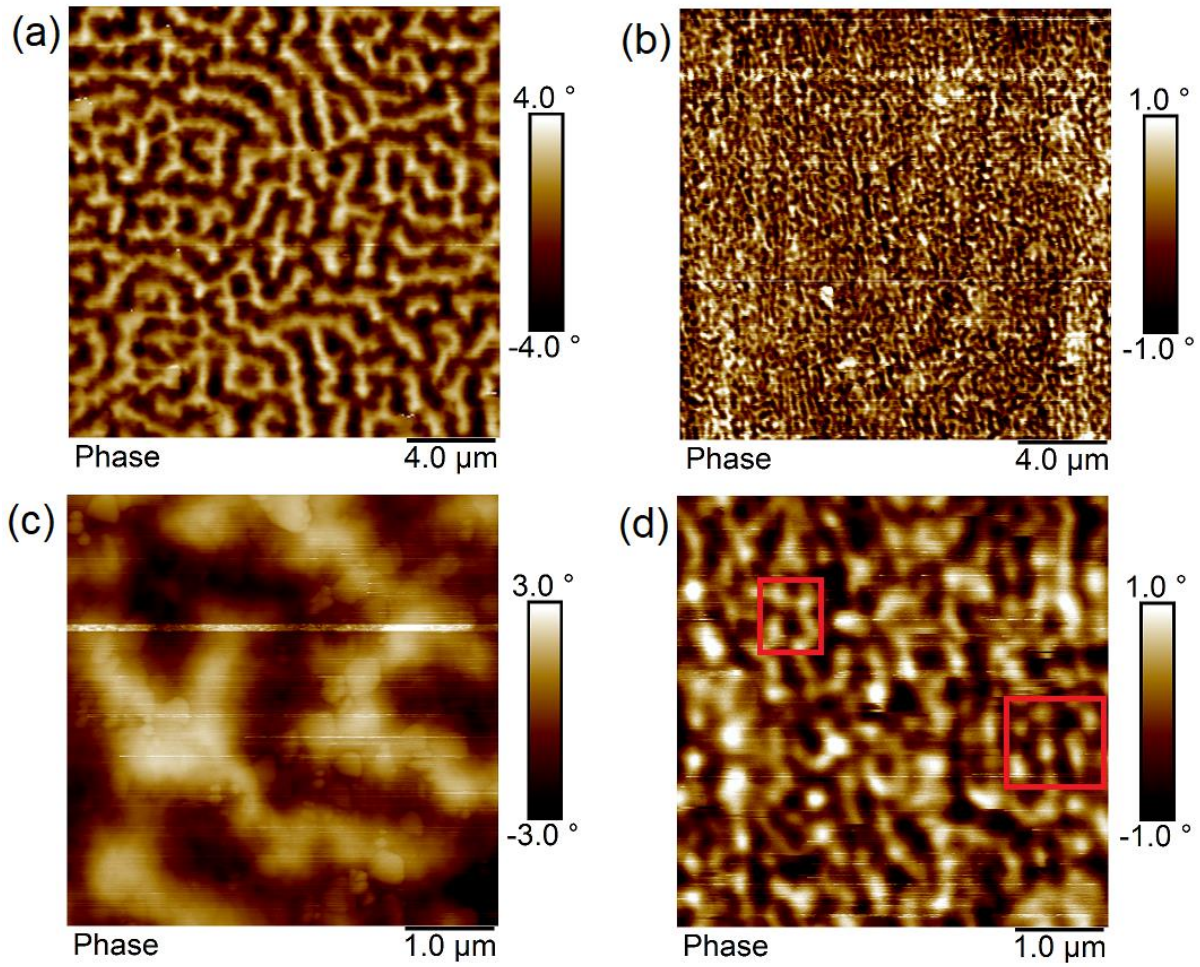

Fig. 6. *MFM image of AL1.5 (a),(c) and Al1.0 (b),(d) samples at different magnification. Total figure size 20 µm x 20 µm (a),(b) and 5 µm x 5 µm (c),(d).*

The results align with the concept that the NPs cluster formation determines the magnetic properties of the samples. It is known that a labyrinth structure of self patterned lamellae stripes is achieved by competing interactions favouring spatial inhomogeneity, governed by the frustrated nature of the interactions. In our case, as the temperature decreases from LTT < T < HTT to T < LTT the new magnetic-bridge provided by the matrix increases the FM-short-range interaction and the formation of Spin-up/Spin-down rich areas is favoured. However, predominant exchange FM interact in Al1.0 larger NPs increases the long-range repulsion that must be balanced to the short-range attraction, resulting in a decrease in the domain size as the repulsion energy is minimized by creating more interfaces. As a consequence, the stripe width decreases with the increase of the relative strength of the short-range FM interaction [37][46]. Thus competing short-range FM interactions and long-range repulsion will determine the domain structure. Hence, weaker dipolar interaction enhance the stripes thickness (sample Al1.5; fig. 6(a)) in the labyrinth structure, whilst a checkerboard pattern is favoured if the long-range repulsive interactions are the predominant interactions (sample Al1.0; fig. 6(b)). No ideal checkerboard pattern should be expected in the Al1.0 sample due to the disorder in particle distribution. However, the appearance of short range local order of both AFM and FM regions arising from disorder and frustrated areas of the size of interparticle's distance is observed in the Al1.0 sample (see red boxed areas in fig. 6(b)). Similar to a SSG-state like of NPs, where the role of the long-range inter-clusters repulsion interactions lead over the short range FM inter-particles interactions.

The mechanism for interparticle interaction inducing a collective behaviour of NPs-clusters have been proven effective for relative low applied fields. At higher fields a detriment in the coupling lead to a behaviour dominated by the single particle anisotropy [35], explaining the AFM-like linear *M(H)* dependence observed in the hysteresis loops for $\mu_0 H > 0.2$ T (fig. 4). For high fields, NPs in a metastable cluster configuration, which are antiparallel aligned to the applied field, will start to respond independently, and the rotation/magnetisation reversal, is favoured. Therefore, as the field increases, more NPs will contribute to the total magnetisation in the direction of the applied field. It also explains why *M(T)* measured at high field (1.0 T) on FC-FH curves are close to the indirect MT measurement as compared to those measured at $\mu_0 H < 50$ mT (fig. 5).

From fig. 5(c). it is noted that the addition of PM-Al element in the NiCoFeCr (Al0.0) starting alloy has improved the saturation magnetisation of the FM-phase. However, the heightening is more pronounced in the Al1.0 sample than in the Al1.5 sample. It has been shown that the higher tendency of the NPs in the Al1.0 sample to form strong FM coupling than in the Al1.5 sample, with the corresponding magnetisation increase. At high applied fields, for greatly independent NPs in the Al1.5 sample, the total saturation magnetisation should be closer to that of the sample Al0.0 as the magnetic moment is carried by the unchanged amount of Fe, Cr and Co elements and no significant enhancement of the magnetisation is expected due to the negligible magnetic NPs interaction. On the other hand, the strong short-order FM exchange interaction between NPs in the Al1.0 sample frustrate the de-coupling of NPs' behaviours at high applied fields.

Analysis: Magnetocaloric effect.

Fig. 7 shows the magnetic entropy change ΔS_m across LTT and HTT of the Al_x samples, where x = 0.0, 1.0 and, 1.5. As expected for a FOPT-like transition (with an irreversible component), ΔS_m^{peak} values are an order of magnitude higher for the HTT transition compared to the LTT transition.

As for the LTT transition, the first thing to notice is the decrease in the size of the ΔS_m^{peak} with the increase of the probability of the samples to form strong FM short-range coupled clusters. Both Al_x samples have lower ΔS_m^{peak} values than Al0.0. i.e. ΔS_m^{peak}(Al0) > ΔS_m^{peak}(Al1.5) > ΔS_m^{peak}(Al1.0). The previously discussed higher magnetic jump associated in the LTT for the Al1.0 sample contrasts with the lower ΔS_m observed. Whilst the total magnetisation increases as consequence of the strong FM-exchange interparticle interaction (enhanced in Al1.0 sample), self-organisation of particles in cluster have been reported to decrease the field induced caloric response of a material [47] as magnetic clusters reduces the magnetic anisotropy.

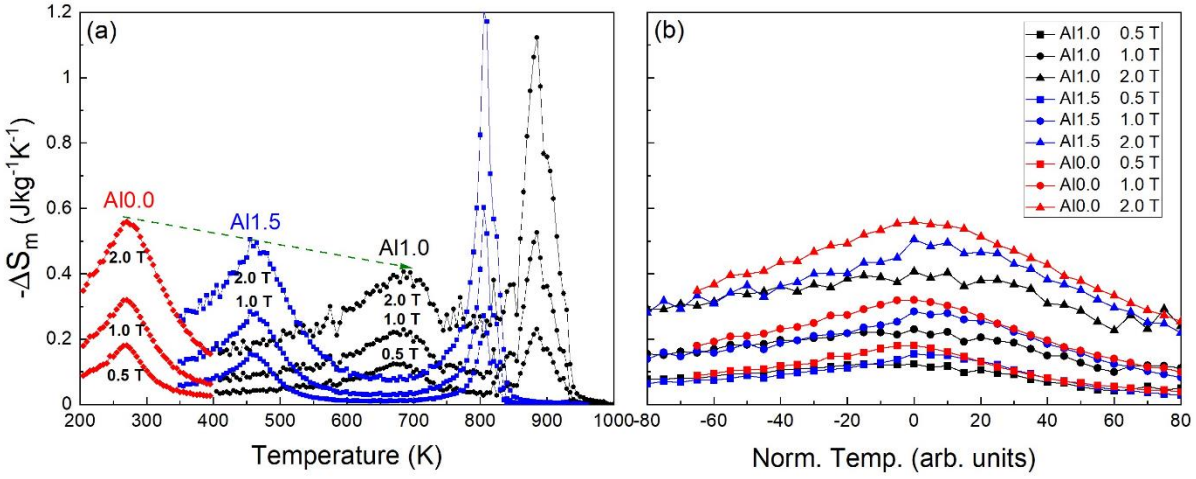

Fig. 7. ΔS_m vs temperature across the LTT and HTT transition **(a)** for applied field of 0.5 T, 1.0 T and, 2.0 T. ΔS_m vs normalized temperature across the LTT transition peaks **(b)**.

The decrease in the ΔS_m^{peak} is accompanied by a broadening of the transition. As a consequence, it is possible to observe a flattening of the transition as the formation of FM clusters is enhanced (fig. 7(b)). Such flattening mirrors what is expected in systems with graded T_C distribution. In this case, a complex dynamic equilibrium between co-existing multiple metastable NPs-clusters might be suggested as the origin of the flattening effect on ΔS_m. For instance, a scaled universal magnetic entropy change curve was plotted in order to study the phase's contribution to the LTT transition (fig. 8.), in which, the second order character of the transition at LTT is confirmed, as the ΔS_m curves obtained at different applied fields collapsed [48]. And, it is observed a uniform displacement of the HTT-peaks with field towards LTT, suggesting a gradually evolvement for different phases.

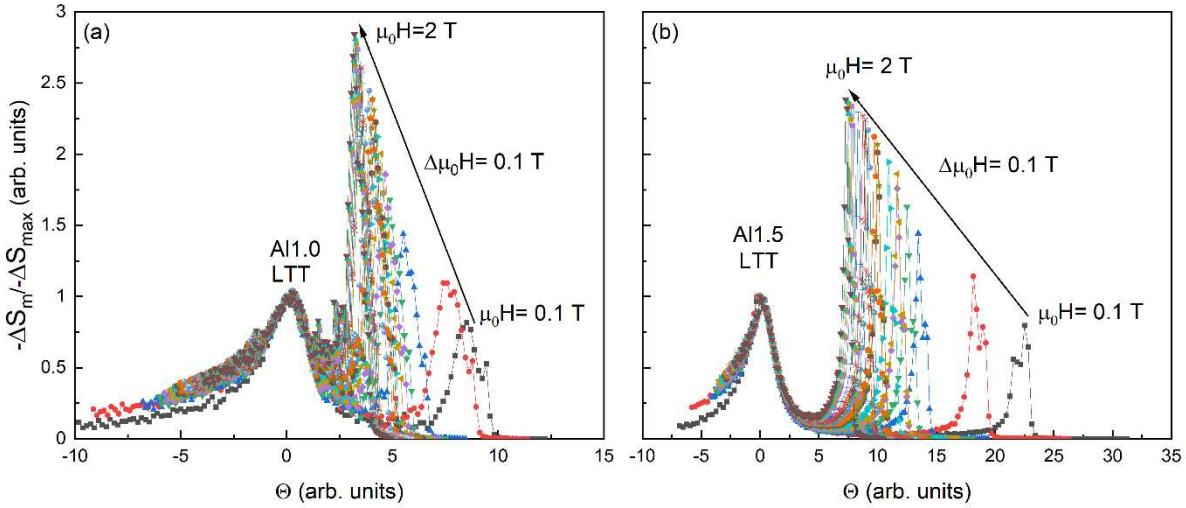

Fig. 8. Universal magnetic entropy change curve: Normalized magnetic entropy change for LTT as a function of the rescaled temperature Θ for sample Al1.0 **(a)** and Al1.5 **(b)**

The augmented practical working temperature range (δT_{FWHM}) provokes an increase in the refrigerant capacity (RC) of the Al1.0 sample as compared to the Al1.5 sample, despite the drop in ΔS_m^{peak}. Calculated RC for the Al1.0 and Al1.5 samples are shown in table.2., where RC=(IΔS_m^{peak}I x δT_{FWHM}) and $\delta T_{FWHM} = T_{hot}$-$T_{cold}$. As such, δT_{FWHM} was found equal to 80 K, 120 K and 150 K for the Al1.5 sample, at $\mu_0\Delta H$ = 0.5 T, 1.0 T and 2.0 T, respectively. As for the Al1.0 sample, high values of ΔS_m for LTT < T < HTT (for instance see fig. 7(b) for norm-T > 60 K) didn't allow for a good estimation of δT_{FWHM}. Therefore, a conservative approach was adopted and approximated δT_{FWHM} to 155 K. i.e. for a temperature window that range from 590 K to 745 K in the $\Delta S_m(T)$ curve (fig. 7(a)), or, from -95 K to 60 K in fig. 7(b). In Al0.0 and Al1.5 samples, ΔS_m tends to zero for $T > T_C$ (PM region) and LTT < T < HTT (SPM-like phase), respectively, as we would expect for a temperature window with few, if any, changes in the magnetic order. On the other hand, the Al1.0 sample tends to keep "a relative high" ΔS_m values for LTT < T < HTT. This can be associated with the SSG-like configuration of NPs and the entropy change associated to cluster re-arrangement between degenerated magnetic states whilst approaching LTT from HTT.

Table 3. shows the ΔS_m^{peak}, RC, and T_{peak} values of the LTT transition for our samples, as well as, for other HEAs reported in bibliography. Notice that ΔS_m^{peak} and RC values corresponding to our Al0.0 sample are amongst the highest reported for HEAs within the room temperature range ($T_C \approx 300$ K) or below. What is more important, T_{peak} was substantially shifted to higher temperatures from 270 K (Al0.0) to T_{peak}^{LTT} = 685 K and 455 K with Al1.0 and Al1.5 additions, respectively. As discussed in [49],

the possibility of tuning T_C whilst keeping the MC properties of a material fairly constant have been one of the most under-studied properties when improving MC-materials performance.

Table. 3. Measured ΔS_m^{peak} and calculated RC values (at LTT) for Al1.0 and Al1.5 samples at different applied fields. Current work and data taken from bibliography for comparison purposes.

sample	$\mu_0\Delta H$ (T)	ΔS_m^{peak} (Jkg^{-1}K^{-1})	RC (Jkg^{-1})	T_{peak} (K)	Ref.
Al0.0	0.5	0.18	16.2[1]	270	Present work
Al1.0	0.5	0.12	18.6[1]	685	Present work
Al1.5	0.5	0.16	12.8[1]	455	Present work
FeCoNiCuMn	0.5	0.115	16.5[1]	395	[19]
$FeCoNiCu_{0.975}Mn_{1.025}$	0.55	0.094	15.3[1]	321	[19]
$FeCoNiCu_{0.95}Mn_{1.05}$	0.55	0.10	13.5[1]	297	[19]
$FeCoNiCu_{0.925}Mn_{1.075}$	0.55	0.084	12.2[1]	279	[19]
$FeCoNiCu_{0.90}Mn_{1.10}$	0.55	0.081	9.6[1]	264	[19]
$Fe_{0.975}CoNiCuMn_{1.025}$	0.55	0.105	14.0[1]	299	[19]
$Fe_{0.950}$ $CoNiCuMn_{1.05}$	0.55	0.071	10.0[1]	292	[19]
FeCoNiCuMn	0.55	< 1.0	-	400	[20]
FeCoNiCuPt	0.55	< 0.2	-	864	[20]
FeCoNiCuMo	0.55	< 0.02	-	657	[20]
Al0.0	1.0	0.32	>36.8[1]	270	Present work
Al1.0	1.0	0.22	34.2[1]	685	Present work
Al1.5	1.0	0.28	33.6[1]	455	Present work
FeCoNiCrAl	1.0	< 0.15	36[1]	290	[50]
NiFeCoCr	1.0	-	< 36[2]	< 100	[21]
$NiFeCoCrPd_{0.12}$	1.0	-	< 36[2]	< 200	[21]
$NiFeCoCrPd_{0.25}$	1.0	-	36[2]	< 250	[21]
[3]$(Fe_{0.76}B_{0.24})_{96}Nb_4$	1.5	1.51	121[1]	559	[51]
[3]$(Fe_{0.75}Tm_{0.01}B_{0.24})_{96}Nb_4$	1.5	1.39	108[1]	537	[51]
[3]$(Fe_{0.71}Tm_{0.05}B_{0.24})_{96}Nb_4$	1.5	1.21	91[1]	450	[51]
[3]$(Fe_{0.66}Tm_{0.10}B_{0.24})_{96}Nb_4$	1.5	1.00	76[1]	390	[51]
[3]$(Fe_{0.59}Tm_{0.17}B_{0.24})_{96}Nb_4$	1.5	0.91	59[1]	316	[51]
[3]$(Fe_{0.58}Tm_{0.18}B_{0.24})_{96}Nb_4$	1.5	0.87	57[1]	325	[51]
Al0.0	2.0	0.56	>75.6[1]	270	Present work
Al1.0	2.0	0.40	62.0[1]	685	Present work
Al1.5	2.0	0.50	75.0[1]	455	Present work
$FeCoNi_{1.05}Cr_{0.95}Al$	2.0	0.27	-	150	[50]
FeCoNiCrAl	2.0	< 0.3	-	290	[50]
$Mn_{27}Cr_7Ni_{33}Ge_{25}Si_8$	2.0	2.49	73.6[1]	412	[52]
NiFeCoCr	5.0	< 0.80	< 100[2]	< 100	[21]
$NiFeCoCrPd_{0.12}$	5.0	< 0.80	< 140[2]	< 200	[21]
$NiFeCoCrPd_{0.25}$	5.0	< 0.90	< 140[2]	< 250	[21]

[1] RC=($I\Delta S_m^{peak}I$ x δT_{FWHM}); [2] RC=($\int_{T_{cold}}^{T_{hot}} -\Delta S_M \, dT$); [3]metallic glass

Although our ΔS_m^{peak} values are an order of magnitude lower than those reported for FeCoNiCuMn [20], $(Fe_{0.76+x}Tm_{0.0-x}B_{0.24})_{96}Nb_4$ [51] and, $Mn_{27}Cr_7Ni_{33}Ge_{25}Si_8$ [52], the comparison to the work here should be made with caution. For instance, $(Fe_{0.76+x}Tm_{0.0-x}B_{0.24})_{96}Nb_4$ is of the metallic glass type, $Mn_{27}Cr_7Ni_{33}Ge_{25}Si_8$ future a *Pnma* space structure [52] and magnetic properties as of the FOPT MnCoGe and MnNiGe type of materials [7] [53] and, the $\Delta S_m(T)$ shape of FeCoNiCuMn-system in [20] reseambles what we obtain at HTT. The lack of analysis for T < 300 K does not allow a full comparison to be made. The ΔS_m^{peak} of about 2.5 Jkg^{-1}K^{-1} measured at $\mu_0\Delta H$ = 2.0 T and HTT at both of our Al_x

samples are of the size of the previously discussed samples found in the literature, and agrees with what we would expect for concomitant transitions as the ones of the first order.

In this study, thanks to the materials functionalisation due to the AlNiCo-FeCr phase separation a competitive MC-response was tuned in a wide temperature region (> 400 K). This demonstrates the ability to achieve a table-like ΔS_m in a single composition by means of tuning its metastable microstructure. As such, we propose a simple materials engineering technique that will allow materials for MC applications to be designed that span from room temperature commercial technologies to high temperature applications such as engines and aircraft cooling systems with no access to cold heat sinks [54].

Conclusions

Following a phenomenological approach, it was successfully explained how by mean of phase separation of the $CoFeNi_{0.5}Cr_{0.5}$-Al_x system into AlNiCo and FeCr rich regions with aluminium addition there is a significant enhancement of the magnetic properties of MC materials. Enhanced saturation magnetisation at T< LTT was explained by means of the collaborative behaviour of segregated FeCr-NPs. It was suggested that a cluster like behaviour of FeCr-rich NPs determines the total magnetisation of $CoFeNi_{0.5}Cr_{0.5}$-Al_x (x = 1.0 and 1.5) where the correlation between NPs-size and magnetisation is as follow:

1- FM-NPs of FeCr rich phase forms at HTT. 2- As the temperature decreases, with the decrease of the thermal energy in the region of LTT < T < HTT, dipolar interaction amongst NPs is favoured for particles of larger size (i.e., Al1.0 sample). Un-favoured NPs' interactions in Al1.5 sample show a SPM-like collective behaviour were NPs are weakly linked to their neighbour. 3- as the sample reaches LTT, the matrix becomes FM and provides the conditions to form the exchange-bridge that will enhanced FM-NPs interaction via the formation of DWs. As consequence, already strong linked NPs of Al1.0 sample increases the FM-like short-range interactions, which in turn increases the long term dipolar repulsion that forms highly fragmented AFM-like domain structure to minimize the energy of the system. On the other hand, the smaller NPs of Al1.5 sample are weakly ferromagnetically aligned which in turn decreases the long-range dipolar repulsions interactions and allows for a wider stripes labyrinth domain structure to form. Note that, clusters formation might happen both before (Al1.0) and during (Al1.5) LTT, thus, depending on the nature of the interparticle interaction.

It was also found that a collaborative behaviours of NPs tents to flatten the magnetic entropy change response to a varied field whilst improve the refrigerant capacity associated to the LTT transition. Relatively large magneto-caloric properties with an enhanced table-like shape were found for the high temperature spectrum, T >> 450 K for Al1.0 and Al1.5 samples. A RC of 17.1 Jkg^{-1} (at $\mu_0\Delta H$ = 1.0 T) and a ΔS_m^{peak} = 0.22 $Jkg^{-1}K^{-1}$ at LTT = 685 K seats on the top of the MC materials that aims to tackle high temperature range of applications such as energy harvesting.

Acknowledgements

This work was supported by the Royal Society Mid-Career Leverhulme Trust Fellowship scheme (SRF\R1\180020) and the Leverhulme Trust (RPG-2018-324)

Data availability statement

The data that support the findings of this study are available from the corresponding author, upon reasonable request.

References

[1] E. Agurgo Balfour *et al.*, "Table-like magnetocaloric effect in Gd56Ni15Al27Zr2 alloy and its field independence feature," *J. Appl. Phys.*, vol. 118, no. 12, p. 123903, 2015.

[2] C. Romero-Muñiz, V. Franco, and A. Conde, "Influence of magnetic interactions between phases on the magnetocaloric effect of composites," *Appl. Phys. Lett.*, vol. 102, p. 082402, 2013.

[3] Y. X. Wang *et al.*, "Outstanding Comprehensive Performance of La(Fe, Si)13Hy/In Composite with Durable Service Life for Magnetic Refrigeration," *Adv. Electron. Mater.*, vol. 4, p. 1700636, 2018.

[4] Y. Shao *et al.*, "High-performance solid-state cooling materials: Balancing magnetocaloric and non-magnetic properties in dual phase La-Fe-Si," *Acta Mater.*, vol. 125, pp. 506–512, 2017.

[5] A. Kitanovski, "Energy Applications of Magnetocaloric Materials," *Adv. Energy Mater.*, vol. 10, no. 10, 2020.

[6] A. Quintana-Nedelcos, J. L. Sánchez Llamazares, and H. Flores-Zuñiga, "On the magnetostructural transition in MnCoGeBx alloy ribbons," *J. Alloys Compd.*, vol. 644, pp. 1003–1008, 2015.

[7] G. Daniel-Pérez *et al.*, "Transformation behavior and magnetocaloric effect in Mn1−xCrxCoGe (x = 0.04 and 0.11) melt-spun ribbons tailored by heat treatment," *J. Magn. Magn. Mater.*, vol. 444, pp. 263–269, 2017.

[8] P. Álvarez, P. Gorria, J. L. Sánchez Llamazares, and J. A. Blanco, "Searching the conditions for a table-like shape of the magnetic entropy in magneto-caloric materials," *J. Alloys Compd.*, vol. 568, pp. 98–101, 2013.

[9] P. Álvarez, J. L. Sánchez Llamazares, P. Gorria, and J. A. Blanco, "Enhanced refrigerant capacity and magnetic entropy flattening using a two-amorphous FeZrB(Cu) composite," *Appl. Phys. Lett.*, vol. 99, p. 232501, 2011.

[10] H. X. Shen *et al.*, "Enhanced refrigerant capacity in Gd-Al-Co microwires with a biphase nanocrystalline/amorphous structure," *Appl. Phys. Lett.*, vol. 108, p. 092403, 2016.

[11] Y. Bao *et al.*, "Table-like magnetocaloric behavior and enhanced cooling efficiency of a Bi-constituent Gd alloy wire-based composite," *J. Alloys Compd.*, vol. 764, pp. 789–793, 2018.

[12] S. Chen *et al.*, "Magnetic transition and magnetocaloric effect of Gd 4 Sb 3-x R x (R=Si, Ge, Sn, 0 ≤ x ≤ 0.75) compounds," *AIP Adv.*, vol. 9, p. 035206, 2019.

[13] A. Quintana-Nedelcos, J. L. S. Llamazares, D. Ríos-Jara, A. G. Lara-Rodríguez, and T. García-Fernández, "Effect of quenching rate on the average grain size and martensitic transformation temperature in rapidly solidified polycrystalline Ni 50Mn37Sn13 alloy ribbons," *Phys. Status Solidi Appl. Mater. Sci.*, vol. 210, pp. 2159–2165, 2013.

[14] V. Chaudhary, X. Chen, and R. V. Ramanujan, "Iron and manganese based magnetocaloric materials for near room temperature thermal management," *Prog. Mater. Sci.*, vol. 100, pp. 64–98, 2019.

[15] Y. F. Wang, F. X. Qin, Y. Luo, H. Wang, and H. X. Peng, "Tuning of magnetocaloric effect and optimization of scaling factor for Gd55Ni10Co35 amorphous microwires," *J. Alloys Compd.*, vol. 761, pp. 1–7, 2018.

[16] J. L. S. Llamazares, A. Quintana-Nedelcos, D. Ríos-Jara, C. F. Sánchez-Valdes, T. García-

Fernández, and C. García, “The effect of low temperature thermal annealing on the magnetic properties of Heusler Ni-Mn-Sn melt-spun ribbons,” *J. Magn. Magn. Mater.*, vol. 401, pp. 38–43, 2016.

[17] Z. Fu *et al.*, “A high-entropy alloy with hierarchical nanoprecipitates and ultrahigh strength,” *Sci. Adv.*, vol. 4, p. eaat8712, 2018.

[18] S. Huang, E. Holmström, O. Eriksson, and L. Vitos, “Mapping the magnetic transition temperatures for medium- and high-entropy alloys,” *Intermetallics*, vol. 95, pp. 80–84, 2018.

[19] A. Perrin, M. Sorescu, M. T. Burton, D. E. Laughlin, and M. McHenry, “The Role of Compositional Tuning of the Distributed Exchange on Magnetocaloric Properties of High-Entropy Alloys,” *J. Miner. Met. Mater. Soc.*, vol. 69, no. 11, pp. 2125–2129, 2017.

[20] M. Kurniawan, A. Perrin, P. Xu, V. Keylin, and M. McHenry, “Curie Temperature Engineering in High Entropy Alloys for Magnetocaloric Applications,” *IEEE Magn. Lett.*, vol. 7, p. 6105005, 2016.

[21] D. D. Belyea, M. S. Lucas, E. Michel, J. Horwath, and C. W. Miller, “Tunable magnetocaloric effect in transition metal alloys,” *Sci. Rep.*, vol. 5, p. 15755, 2015.

[22] N. A. Morley, C. R. B. Lim, J. Xi, A. Quintana-Nedelcos, and Z. Leong, “Magnetic Properties of the Complex Concentrated Alloy System CoFeNi 0.5 Cr 0.5 Al,” *Sci. Rep.*, vol. 10, p. 14506, 2020.

[23] D. T. Hong Gam, N. H. Hai, L. Van Vu, N. H. Luong, and N. Chau, “The existence of large magnetocaloric effect at low field variation and the anti-corrosion ability of Fe-rich alloy with Cr substituted for Fe,” *J. Phys. Conf. Ser.*, vol. 187, p. 012067, 2009.

[24] N. Chau, P. Q. Thanh, N. Q. Hoa, and N. D. The, “The existence of giant magnetocaloric effect and laminar structure in Fe73.5-xCrxSi13.5 B9Nb3Cu1,” *J. Magn. Magn. Mater.*, vol. 304, pp. 36–40, 2006.

[25] C. Zhang, Y. Li, X. H. Han, S. long Du, J. bing Sun, and Y. Zhang, “Structure and magnetic properties of Alnico ribbons,” *J. Magn. Magn. Mater.*, vol. 451, pp. 200–207, 2018.

[26] L. Zhou *et al.*, “Architecture and magnetism of alnico,” *Acta Mater.*, vol. 74, pp. 224–233, 2014.

[27] M. C. Nguyen, X. Zhao, C. Z. Wang, and K. M. Ho, “Cluster expansion modeling and Monte Carlo simulation of alnico 5-7 permanent magnets,” *J. Appl. Phys.*, vol. 117, no. 9, p. 093905, 2015.

[28] N. I. Kulikov, “Onset of magnetism in B 2 transition-metal aluminides,” *Phys. Rev. B*, vol. 59, no. 10, pp. 6824–6833, 1999.

[29] R. Kulkarni, B. S. Murty, and V. Srinivas, “Study of microstructure and magnetic properties of AlNiCo(CuFe) high entropy alloy,” *J. Alloys Compd.*, vol. 746, pp. 194–199, 2018.

[30] X. H. Han, J. B. Sun, H. W. Wang, Z. X. Dong, Y. Zhang, and C. X. Cui, “Excellent magnetic properties determined by spinodal decomposition structure of Alnico alloy doped SmCo5-based ribbons,” *J. Alloys Compd.*, vol. 806, pp. 1188–1199, 2019.

[31] Y. Duan, X. Wen, B. Zhang, G. Ma, and T. Wang, “Optimizing the electromagnetic properties of the FeCoNiAlCrx high entropy alloy powders by composition adjustment and annealing treatment,” *J. Magn. Magn. Mater.*, vol. 497, p. 165947, 2020.

[32] S. Öztürk, K. İçin, M. Gençtürk, M. Göbülük, and P. Svec, “Effect of heat treatment process on

the structural and soft magnetic properties of Fe38Co38Mo8B15Cu ribbons," *J. Non. Cryst. Solids*, vol. 527, p. 119745, 2020.

[33] C. Antoniak *et al.*, "Composition dependence of exchange stiffness in FexPt 1-x alloys," *Phys. Rev. B*, vol. 82, p. 064403, 2010.

[34] B. F. O. Costa, J. Cieslak, and S. M. Dubiel, "Anomalous behaviour of the Debye temperature in Fe-rich Fe-Cr alloys," *J. Alloys Compd.*, vol. 492, pp. L1–L4, 2010.

[35] G. Muscas *et al.*, "The interplay between single particle anisotropy and interparticle interactions in ensembles of magnetic nanoparticles," *Phys. Chem. Chem. Phys.*, vol. 20, no. 45, pp. 28634–28643, 2018.

[36] D. Kecharakos and K. N. Trohidou, "Competition between dipolar and exchange interparticle interactions in magnetic nanoparticle films D. Kechrakos and K. N. Trohidou Institute of materials Science, NCSR 'Demokritos', Aghia Paraskevi, 15310 Athens, Greece," *J. Magn. Magn. Mater.*, vol. 262, pp. 107–110, 2003.

[37] A. Magni, "Hysteresis properties at zero temperature in the dipolar random-field ising model," *Phys. Rev. B*, vol. 59, no. 2, pp. 985–990, 1999.

[38] J. L. Dormann, D. Fiorani, and E. Tronc, "On the models for interparticle interactions in nanoparticle assemblies: comparison with experimental results," *J. Magn. Magn. Mater.*, vol. 202, no. 1, pp. 251–267, 1999.

[39] S. Mørup, M. F. Hansen, and C. Frandsen, "Magnetic interactions between nanoparticles," *Beilstein J. Nanotechnol.*, vol. 1, no. 1, pp. 182–190, 2010.

[40] R. Díaz-Méndez, G. Pupillo, F. Mezzacapo, M. Wallin, J. Lidmar, and E. Babaev, "Phase-change switching in 2D: Via soft interactions," *Soft Matter*, vol. 15, no. 3, pp. 355–358, 2019.

[41] S. Das, P. Ranjan, P. S. Maiti, G. Singh, G. Leitus, and R. Klajn, "Dual-responsive nanoparticles and their self-assembly," *Adv. Mater.*, vol. 25, pp. 422–426, 2013.

[42] D. Peddis, F. Orrù, A. Ardu, C. Cannas, A. Musinu, and G. Piccaluga, "Interparticle interactions and magnetic anisotropy in cobalt ferrite nanoparticles: Influence of molecular coating," *Chem. Mater.*, vol. 24, pp. 1062–1071, 2012.

[43] S. Sahoo *et al.*, "Magnetic relaxation phenomena in the superspin-glass system [Co80Fe20/Al2O3]10," *J. Phys. Condens. Matter*, vol. 14, no. 26, pp. 6729–6736, 2002.

[44] A. Quintana-Nedelcos *et al.*, "On the correct estimation of the magnetic entropy change across the magneto-structural transition from the Maxwell relation: Study of MnCoGeBxalloy ribbons," *J. Alloys Compd.*, vol. 694, pp. 1189–1195, 2017.

[45] A. K. Gangopadhyay, H. Krishna, C. Favazza, C. Miller, and R. Kalyanaraman, "Heterogeneous nucleation of amorphous alloys on catalytic nanoparticles to produce 2D patterned nanocrystal arrays," *Nanotechnology*, vol. 18, p. 485606, 2007.

[46] Y. Mu and Y. Q. Ma, "Stripe patterns in frustrated spin systems," *J. Chem. Phys.*, vol. 117, no. 4, pp. 1686–1691, 2002.

[47] L. C. Branquinho *et al.*, "Effect of magnetic dipolar interactions on nanoparticle heating efficiency: Implications for cancer hyperthermia," *Sci. Rep.*, vol. 3, p. 2887, 2013.

[48] J. Y. Law *et al.*, "A quantitative criterion for determining the order of magnetic phase transitions using the magnetocaloric effect," *Nat. Commun.*, vol. 9, no. 1, pp. 1–9, 2018.

[49] A. Quintana-Nedelcos, J. L. Sánchez Llamazares, and G. Daniel-Perez, "Enhanced magnetocaloric effect tuning efficiency in Ni-Mn-Sn alloy ribbons," *J. Magn. Magn. Mater.*, vol. 441, pp. 188–192, 2017.

[50] S. M. Na, P. K. Lambert, H. Kim, J. Paglione, and N. J. Jones, "Thermomagnetic properties and magnetocaloric effect of FeCoNiCrAl-type high-entropy alloys," *AIP Adv.*, vol. 9, p. 035010, 2019.

[51] J. Li *et al.*, "Magnetocaloric effect in Fe-Tm-B-Nb metallic glasses near room temperature," *J. Non. Cryst. Solids*, vol. 425, pp. 114–117, 2015.

[52] K. Sarlar, A. Tekgul, and I. Kucuk, "Magnetocaloric properties of rare earth free Mn27Cr7Ni33Ge25Si8 High Entropy Alloy," *IEEE Magn. Lett.*, vol. 10, p. 2109905, 2019.

[53] G. Daniel-Pérez, J. L. Sánchez Llamazares, A. Quintana-Nedelcos, P. Álvarez-Alonso, R. Varga, and V. Chernenko, "Magnetostructural transition and magnetocaloric effect in MnNiGe 1.05 melt-spun ribbons," *J. Appl. Phys.*, vol. 115, p. 17A920, 2014.

[54] S. Dey, R. K. Roy, A. Basu Mallick, A. Mitra, and A. K. Panda, "High-temperature magnetocaloric effect in devitrified Fe/Co based glassy monolayer and bilayer ribbons," *J. Mater. Sci.*, vol. 54, no. 16, pp. 11292–11303, 2019.